A Directional Protection Scheme for HVDC Transmission Lines Based on Reactive Energy

Shuxin Luo, *Student Member, IEEE*, Xinzhou Dong, *Senior Member, IEEE*, Shenxing Shi, *Member, IEEE*, and Bin Wang, *Member, IEEE*

***Abstract*—High-voltage direct-current (HVDC) transmission-line protection is becoming increasingly desirable with the expanding worldwide popularity of HVDC technologies in recent years. This paper proposes a transmission-line backup protection scheme based on the integral of reactive power for HVDC systems. The directional characteristics of reactive power flow are theoretically analyzed for internal and external faults, and these characteristics are used to construct a directional protection scheme. The Hilbert transform is adopted to calculate the reactive power, which ensures a continuous output of calculation results and improves the reliability of the protection. A bipolar 12-pulse HVDC test system based on the CIGRE benchmark is modeled using PSCAD/EMTDC, and extensive simulations of various fault situations are conducted to test the effectiveness of the proposed scheme. The simulation results show that the proposed protection scheme correctly identifies internal and external faults and performs well with different fault distances and fault resistances. Furthermore, the proposed protection is insensitive to the sampling frequency, making it practical for future applications.**

***Index Terms*—Directional protection, Hilbert transform, HVDC system, power system protection, reactive energy.**

I. Introduction

With the rapid development of power systems, high-voltage direct-current (HVDC) transmission technology has played an increasingly significant role in recent years. Compared to high-voltage alternating current (HVAC) technology, HVDC technology is more competitive for long-distance power transmission, asynchronous power grid interconnections, and renewable energy integration due to its flexible power control and large power transmission capacity [1], [2]. Among the numerous techniques concerning HVDC, dc transmission-line protection is an important unit in HVDC control and protection systems, as it provides fast fault clearance and guarantees the operation security of the entire HVDC transmission system.

Traditional dc transmission-line protection uses the voltage differential rate to detect the line faults [3], which is sensitive to fault resistance and cannot correctly identify a high-impedance fault. Reference [4] introduces high-speed traveling-wave protection to transmission-line protection, but its performance is easily affected by disturbance. In addition, it has low sensitivity in high impedance fault situations. Distance protection provides another approach to identify the line fault-by-fault distance estimation. References [5]–[7] use the time difference between the initial wave and reflected wave from the fault point to calculate the fault distance, although it is difficult to distinguish the reflected wave from the disturbing waves in some cases. Distance protection based on the Bergeron transmission-line model is developed in [8]. However, measurement errors cannot be avoided in this method and, thus, the protection zone cannot reach the entire length of the dc line. Recently, studies have reported boundary protection using single terminal data [9]–[11]. Internal and external faults are clearly discriminated based on the frequency characteristics of the line boundary components, including the smoothing reactor and dc filters. However, most of these protection methods require a high-frequency sampling rate, which is not practical in many applications.

Transmission-line backup protection is imperative in cases when the primary protection fails. DC minimum voltage protection is widely applied in practice due to its simplicity [3]. However, it has no selectivity between dc line faults and ac system faults. Current differential protection is another solution for HVDC transmission-line backup protection [12]. However, a time delay is essential to prevent maloperation of this type of protection under external fault situations, due to the fluctuating transient current at the beginning of the fault. A delay of 0.5 s is typically introduced to ensure the reliability of the protection [13], which significantly decreases the operating speed of the protection.

This paper proposes a novel directional backup protection scheme based on reactive energy for HVDC transmission systems. In this paper, reactive energy is defined as the integral of reactive power during a period of time. The Hilbert transform is employed to continuously calculate the reactive energy, and then, the reactive energy flow directions are applied to identify internal and external faults. Compared to the traditional current differential scheme, this protection has a smaller time delay, thus significantly increasing the protection speed. Various simulation results indicate that the proposed protection performs well under

Manuscript received December 22, 2014; revised April 05, 2015, June 01, 2015, and June 25, 2015; accepted July 23, 2015. Date of publication July 28, 2015; date of current version March 22, 2016. This work was supported in part by the National Natural Science Foundation of China under Grants 51120175001, 51107062, and 51477084, and in part by the Beijing Natural Science Foundation under Grant 3152016. Paper no. TPWRD-01579-2014.

The authors are with the State Key Laboratory of Control and Simulation of Power System and Generation Equipment, Department of Electrical Engineering, Tsinghua University, Beijing 100084, China (e-mail: luosx10@mails.tsinghua.edu.cn; xzdong@tsinghua.edu.cn; shishenxing@tsinghua.edu.cn; binw_ee@tsinghua.edu.cn).

Color versions of one or more of the figures in this paper are available online at http://ieeexplore.ieee.org.

Digital Object Identifier 10.1109/TPWRD.2015.2461450

various situations, and the sensitivity and reliability of the protection are satisfactory.

The remainder of this paper is organized as follows. In Section II, the reactive energy based on the Hilbert transform is introduced as the key index of the protection, and the features of the reactive energies during different faults are analyzed based on the equivalent circuit of an HVDC system. In Section III, the detailed protection scheme, including the startup component, time delay, threshold settings, and fault pole selection, is presented. A simulation model based on the CIGRE benchmark is built using PSCAD/EMTDC, as described in Section IV, and extensive simulations are conducted to test the effectiveness of the proposed protection. Finally, concluding remarks are presented in Section V.

II. Basic Principle

A. Index for the Protection Principle

Under normal operating situations, HVDC systems mostly transmit active power, whereas the reactive power flow on the dc line is nearly zero except for some small harmonic components. The quantity of the harmonic reactive power on the dc line depends on the filtering effects of the dc filters and the smoothing reactors. The total quantities of the harmonic voltage and current are typically less than 5% of the rated values [14]. However, when a line fault occurs, the voltage and current at the terminals of the DC line will contain a transient component due to the inductive and capacitive components in the system, thus resulting in significant reactive power flows on the dc line.

In traditional HVDC systems, shunt capacitor banks are commonly used for compensating the reactive power which the converters consume. Reactive power control is designed to maintain the reactive power balance by switching the capacitor banks [15]. The consumption of reactive power can only be changed in steps by switching in or out of the capacitor banks. This discrete kind of control needs to be blocked during the transient process to avoid frequent switch operations, and the control speed is typically 10–20 s per step [15]. Thus, the reactive power is considered to be uncontrolled during the fault period, and it is primarily affected by the characteristics of the system components. As analyzed in this section, the uncontrolled reactive power flows from the source to the fault point during the fault transient process, indicating that the reactive power has different directions in internal and external fault situations.

According to the aforementioned analysis, the reactive power on the dc line can be utilized to identify the fault occurrence and distinguish the internal and external faults. Therefore, the integral of reactive power is selected to construct the HVDC line protection in this study.

B. Hilbert Transform-Based Reactive Energy

The Hilbert transform is used to calculate the reactive energy, which is defined as the convolution of $x(t)$ with the function $h(t) = 1/\pi t$ [16], as shown in

$$\hat{x}(t) = x(t) * h(t) = x(t) * \frac{1}{\pi t} = \frac{1}{\pi} \int_{-\infty}^{\infty} \frac{x(\tau)}{t-\tau} d\tau \qquad (1)$$

where $\hat{x}(t)$ is the Hilbert transform result of $x(t)$ and "$*$" is the operator for time-domain convolution.

The frequency characteristic of $h(t)$ is expressed in (2). $h(t)$ induces a -90° shift for positive frequency components and a $+90^\circ$ shift for negative frequency components. Thus, $h(t)$ can be regarded as an all-pass filter except for the dc component

$$H(\omega) = -j\mathrm{sgn}(\omega) = \begin{cases} -j, & \text{for } \omega > 0 \\ 0, & \text{for } \omega = 0 \\ j, & \text{for } \omega < 0 \end{cases}. \qquad (2)$$

For real-time calculations, the Hilbert transform can be discretized as

$$\hat{x}[n] = x[n] * h[n] \qquad (3)$$

where

$$h[n] = \begin{cases} 0, & \text{for } n \text{ even} \\ \frac{2}{n\pi}, & \text{for } n \text{ odd.} \end{cases} \qquad (4)$$

A Hamming window function is used to truncate $h[n]$ for finite calculations in practice.

The instantaneous reactive power is defined as the multiplication of the current signal $i(t)$ and the Hilbert transform of the voltage signal $v(t)$ [17], as shown in

$$q(t) = \hat{v}(t) i(t) \qquad (5)$$

where $\hat{v}(t)$ is the Hilbert transform of the voltage signal $v(t)$.

The reactive energy during a period of time t is calculated as

$$W(t) = \int_0^t q(\tau) d\tau = \int_0^t \hat{v}(\tau) i(\tau) d\tau. \qquad (6)$$

According to [17], it can be proven that the integration of the defined instantaneous reactive power during one cycle is equal to the traditional reactive power definition.

Compared to the traditional calculation method, the algorithm based on the Hilbert transform derives the reactive energy directly from the original sampled voltage and current signals. Thus, it is not necessary to calculate the discrete Fourier transform (DFT) of the voltage and current for the magnitudes and angles of all harmonic components. Furthermore, the proposed method acquires the reactive energy continuously in real time, which accelerates the operation of the protection system, whereas traditional calculation requires a complete cycle of the measured data. Therefore, the reactive energy based on the Hilbert transform is used for protection identification in the following section.

C. Equivalent Circuit of the HVDC System

The HVDC transmission line is connected to ac systems via dc converters. According to the Thévenin equivalent principle, the dc converter with the ac system can be modeled using a dc source and an equivalent impedance at the dc system side, as shown in Fig. 1. U_{dcR} and U_{dcI} are the equivalent dc sources, and Z_{dcR} and Z_{dcI} are the equivalent impedances at the rectifier side and inverter side. Z_S and Z_F represent the smoothing reactor and dc filter, respectively. For a bipolar HVDC system, the positive pole and negative pole operate independently. Thus,

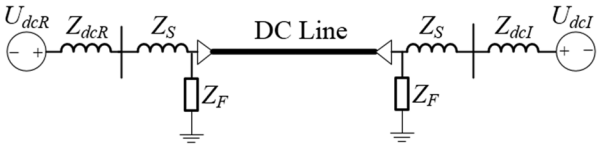

Fig. 1. Equivalent HVDC system on the dc side.

the equivalent system for the bipolar system can be considered as the combination of two monopolar systems.

According to the switch function theory of HVDC converters [18], [19], the equivalent impedances of the 6-pulse ($Z_{\mathrm{dc}-6}$) and 12-pulse ($Z_{\mathrm{dc}-12}$) converter HVDC systems can be calculated as

$$Z_{\mathrm{dc}-6}(\omega) = \frac{9\sin\mu}{\pi^2\mu}\left[Z_{cs}(\omega-\omega_0) + Z_{cs}(\omega+\omega_0)\right] \quad (7)$$

$$Z_{\mathrm{dc}-12}(\omega) = \frac{18\sin\mu}{\pi^2\mu}\left[Z_{cs}(\omega-\omega_0) + Z_{cs}(\omega+\omega_0)\right] \quad (8)$$

where μ is the commutation angle in radians and ω_0 is the angular frequency of the ac power. Z_{cs} denotes the summation of the converter transformer impedance and equivalent impedance of the ac system. According to (7) and (8), Z_{dc} is inductive regardless of variations in frequency.

D. Internal Fault

During the fault transient process, the source of the HVDC system can be regarded as a steady dc voltage source superimposed with a varying harmonic voltage source, as shown in Fig. 2(a), where $\boldsymbol{U}_{hR}$ and $\boldsymbol{U}_{hI}$ are the transient sources generated during a fault situation. X_{L1}, X_{L2}, R_{L1}, and R_{L2} denote the dc transmission-line reactors and resistances, respectively. The harmonic source represents all of the frequency components of the voltage, which are time-variant during the fault transient process. According to the superposition theorem, the system in Fig. 2(a) can be divided into a dc steady state and transient fault state, as shown in Fig. 2(b) and (c). Since reactive power cannot be generated by the steady dc source, it only exists in the harmonic source network.

As shown in Fig. 2(c), regardless of the resistances and capacitances of the transmission line, the reactive power at the rectifier side and inverter side can be expressed as

$$Q_R = \left[\frac{|\boldsymbol{U_{hR}}|Z_F}{(Z_{dcR}+Z_S+X_{L1}//Z_F)(Z_F+X_{L1})}\right]^2 X_{L1} \quad (9)$$

$$Q_I = \left[\frac{|\boldsymbol{U_{hI}}|Z_F}{(Z_{dcI}+Z_S+X_{L2}//Z_F)(Z_F+X_{L2})}\right]^2 X_{L2} \quad (10)$$

where the symbols are defined in Fig. 2.

According to (9) and (10), the reactive power at both sides is positive and flows toward the fault point, as shown in Fig. 2(c).

Therefore, the directions of the reactive power at both sides are opposite during internal faults.

E. External Fault

During external faults, the dc voltage and current also contain transient components and produce reactive energy flow. The external fault network can also be represented by a dc source and a harmonic voltage source network. Fig. 3(a) shows the harmonic

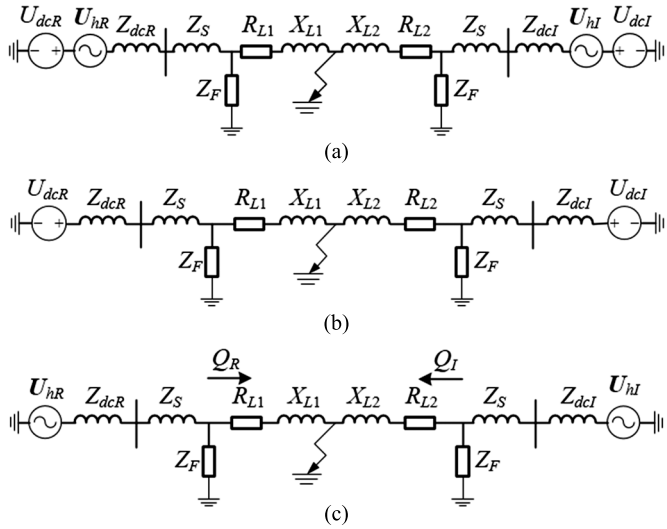

Fig. 2. Equivalent system during internal faults. (a) The entire network. (b) The DC source network. (c) The harmonic source network.

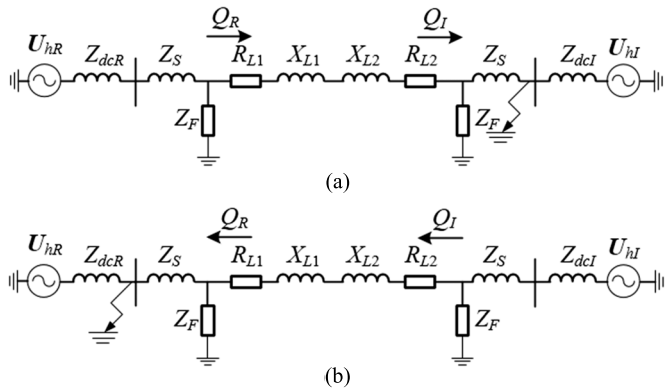

Fig. 3. Reactive energy flow during external faults. (a) Inverter-side fault. (b) Rectifier-side fault.

source network where the fault is located at the inverter side. The reactive power at both sides can be calculated as

$$Q_R = |\boldsymbol{I}_h|^2(X_{L1}+X_{L2}+Z_S//Z_F) \quad (11)$$

$$Q_I = |\boldsymbol{I}_h|^2(Z_F//Z_S) \quad (12)$$

where

$$\boldsymbol{I}_h = \frac{\boldsymbol{U}_{hR}}{[(Z_F//Z_S+X_{L1}+X_{L2})//Z_F+Z_{\mathrm{dc}R}+Z_S]}.$$

The reactive power at both sides flows toward the fault point, which indicates that the reactive power at the rectifier side and inverter side has the same direction during external fault situations, as displayed in Fig. 3(a). The same conclusion is obtained when an external fault occurs at the rectifier side, as shown in Fig. 3(b).

III. Protection Scheme

A. Fault Direction Identification

Directional protection is used for internal and external fault identification in this scheme. In this study, the reference direction of the reactive energy is from the rectifier side to the inverter

side. If the reactive energies of each side have different directions, an internal fault is identified. Otherwise, an external fault is detected. Thus, the fault direction identification criteria can be expressed as

$$\begin{cases} \text{internal fault} : W_R(t)W_I(t) < 0 \\ \text{external fault} : W_R(t)W_I(t) > 0 \end{cases} \tag{13}$$

where W_R and W_I are the reactive energies measured at the rectifier side and inverter side, respectively.

In a monopolar HVDC system, single-pole reactive energy is used for direction identification, whereas in a bipolar system, the sum of the reactive energies at the two poles is used as follows:

$$W(t) = W_{\text{pos}}(t) + W_{\text{neg}}(t) \tag{14}$$

where W_{pos} and W_{neg} are the reactive energies of the positive pole and negative pole, respectively.

B. Startup Component

A protection startup component is introduced to ensure the reliability of the protection scheme in case of disturbances. Once the startup requirement is satisfied, the protection scheme is triggered to start the calculation process. In this study, the dc voltage differential du/dt or current differential di/dt is used as the startup component.

C. Time Delay

Due to the frequent energy exchange between the inductive and capacitive components at the beginning of the fault transient process, the reactive energy varies between positive and negative values, which results in unstable directions during this period. Therefore, a time delay is introduced to prevent fluctuating reactive energy directions. In this study, the time delay is set to two power frequency cycles, which is sufficiently long for a stationary direction outcome.

D. Threshold Setting

A threshold for the reactive energy is necessary to avoid maloperation during disturbances. When the calculated reactive energy is larger than the threshold, the fault direction identification module is activated. The setting value W_{set} is set as

$$W_{\text{set}} = k_r W_{\text{har}} = k_r \cdot (k_{\text{har}} U_N \cdot k_{\text{har}} I_N \cdot t) = k_r k_{\text{har}}^2 U_N I_N t_d \tag{15}$$

where

- k_r reliability coefficient;
- W_{har} reactive energy of the harmonic components;
- k_{har} proportion coefficient of the harmonic voltage and current;
- U_N, I_N rated voltage and current of the HVDC system, respectively;
- t_d delay time.

E. Fault Pole Selection

In a bipolar HVDC transmission system, fault pole selection is essential for the protection scheme in single-pole-to-ground faults to isolate the faulty pole and maintain continuous operation of the healthy pole. Due to the mutual coupling effect of the two poles, the healthy pole may also generate reactive energy during a single-pole-to-ground fault. However, this reactive energy is considerably smaller than that in the faulty pole. Hence, the fault pole selection coefficient is defined in (16), where three types of faults can be classified. When $k \le 1/k_{\text{set}}$, the fault pole is determined as the negative pole, whereas a positive pole fault results when $k \ge k_{\text{set}}$, where k_{set} is the setting threshold of the pole selection coefficient. The fault is considered a bipolar fault when $1/k_{\text{set}} < k < k_{\text{set}}$.

$$k = \left| \frac{W_{\text{pos}}(t)}{W_{\text{neg}}(t)} \right|. \tag{16}$$

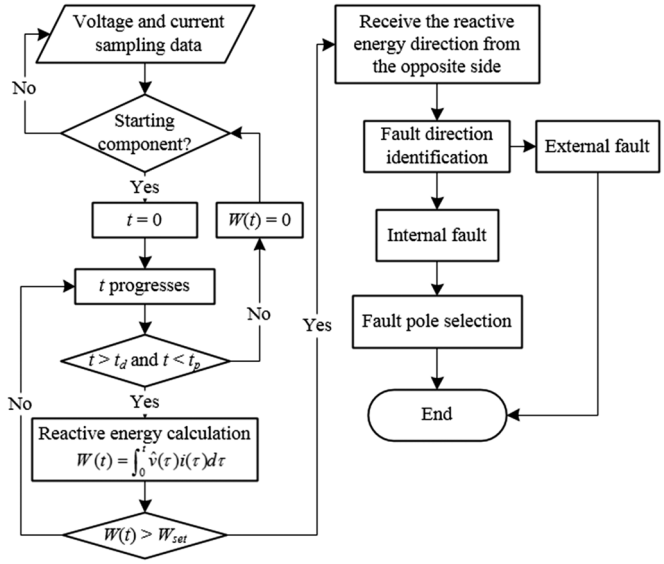

Fig. 4. Flowchart of the protection scheme.

F. Flow Diagram

The integrated flow diagram of the protection scheme is shown in Fig. 4. When the startup condition is satisfied, the time variable t is set to 0. As time progresses, t is incremented. When the time delay is satisfied, the protection scheme begins to calculate the reactive energy from the protection startup time using (6). When t exceeds the protection time t_p, the reactive energy index is reset to 0, and the protection algorithm waits for the next startup. If the calculated reactive energy is larger than the setting threshold, an internal or external fault can be identified according to the reactive energy direction information from the other side. Finally, the faulty pole is selected in the internal fault situation.

G. Discussion

The proposed protection algorithm is a pilot method, which relies on a remote communication link to obtain the reactive energy direction from the opposite side. Thus, various drawbacks, including the signal transfer delay, the cost, and reliability of the communication link, are inevitable for this type of protection.

Currently, optical ground wires (OPGWs) are widely used in HVDC transmission systems [20]. The signal transfer delay in

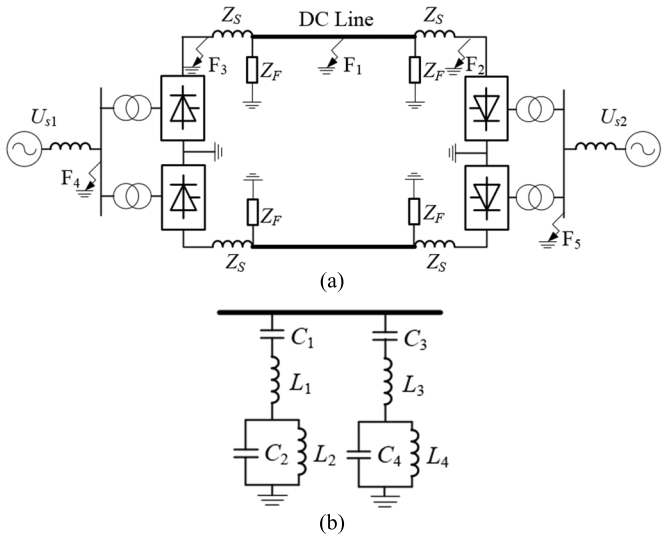

Fig. 5. Bipolar HVDC transmission system. (a) The entire HVDC system. (b) DC filters.

an optical-fiber cable is approximately 4.9 μs/km [21]. Thus, for a 1000-km-long transmission line, the delay time is approximately 5 ms, which is acceptable for a backup protection. Furthermore, this protection can employ existing communication links without additional cost. Regarding the reliability concerns, OPGWs are immune to electromagnetic interference arising from corona on dc wires or faults in the transmission system [20], which ensures high communication reliability. However, the risk of losing the communication link cannot be completely eliminated. Therefore, protection is blocked if the communication link is out of service.

Compared to other pilot protections that are currently in use, for example, current differential protection, the protection scheme proposed in this paper only transfers the reactive energy direction. Thus, less information must be transferred, and a communication link with relatively low speed is acceptable. This feature makes the directional protection scheme more practical than the currently used differential protection systems.

IV. Test System and Simulation Results

A. Test System

A bipolar HVDC system based on the CIGRE benchmark is built using PSCAD/EMTDC in this paper [22], [23]. The structure of the HVDC system is shown in Fig. 5. DC filters are used for the 12th, 24th, and 36th harmonic filtering components. The parameters of the HVDC system are shown in the Appendix. A frequency-dependent transmission-line model is used [24], and the sampling frequency of the dc voltage and current is 10 kHz.

B. Performance

Several fault and disturbance situations are simulated to test the effectiveness of the proposed protection scheme. The protection setting parameters are set as follows. The reliability coefficient k_r is set to 1.5, and the proportion coefficient of the harmonic components k_{har} is 0.05. The delay time t_d is set as 0.04 s, which is equal to two ac frequency cycles. Therefore, the

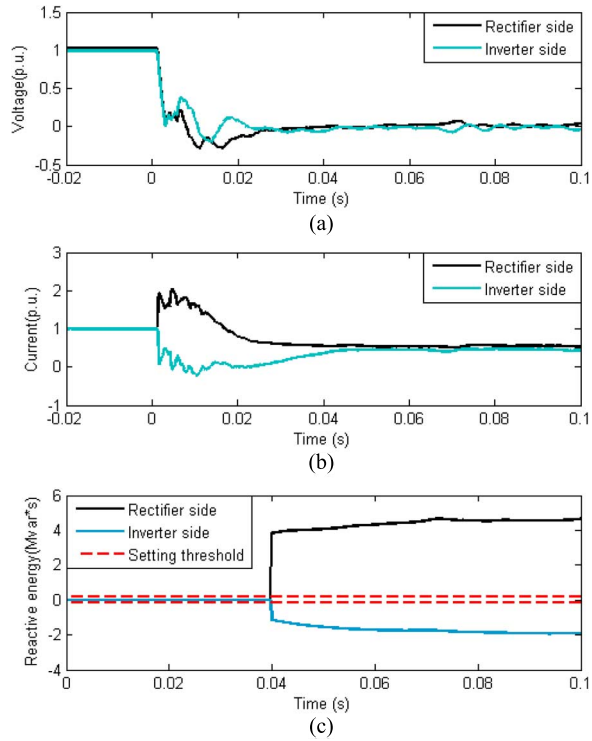

Fig. 6. Simulation results of the dc-line fault. (a) Voltage. (b) Current. (c) Reactive energy.

TABLE I
Simulation Results for Different Fault Types

Fault type	W_R (Mvar*s)	W_I (Mvar*s)	Pole selection coefficient k	Fault identification result
Positive pole fault	3.8290	-1.1483	39.9758	
Negative pole fault	3.8297	-1.1494	0.0250	Internal faults
Bipolar fault	9.9140	-3.8859	1.0008	

reactive energy threshold is calculated as 0.15 Mvar·s according to (15). The setting threshold of the pole selection coefficient is set to 5.

Internal Faults: The dc transmission-line fault is located at F_1 in Fig. 5(a), and a positive pole fault is simulated. The fault distance is 400 km from the rectifier side. The voltage, current, and reactive energies at both sides during the line fault are shown in Fig. 6. The fault occurs at 0 s, and the calculated reactive energies of both sides exceed the threshold immediately after a delay time of 0.04 s. The directions of the reactive energies from two sides are opposite, as previously analyzed, and the direction indication lasts for a long period of time, permitting reliable identification. A negative pole fault and bipolar fault are also simulated. The reactive energies at 0.04 s and the fault pole selection coefficients are listed in Table I. The results show that the proposed protection is adaptive for different fault types, and the fault pole selection method correctly selects the fault type.

DC External Faults: The external faults located at F_2 and F_3 in Fig. 5(a) are simulated, and the simulation results of both sides are displayed in Figs. 7 and 8, respectively. The reactive energies are both positive when the faults occur at the inverter side, whereas they are both negative for the rectifier-side fault.

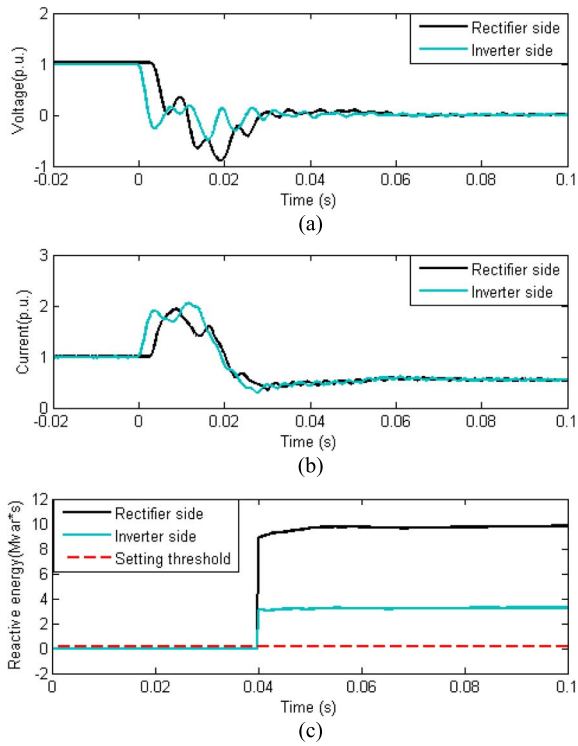

Fig. 7. Simulation results of an inverter-side fault. (a) Voltage. (b) Current. (c) Reactive energy.

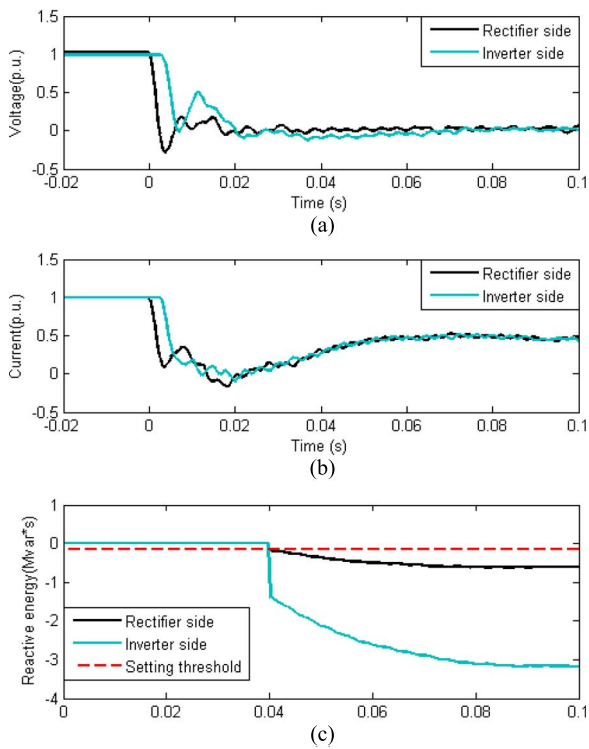

Fig. 8. Simulation results of a rectifier-side fault. (a) Voltage. (b) Current. (c) Reactive energy.

Thus, the directions of the reactive energies at both sides are the same in external fault situations, as analyzed in Section II.

TABLE II
SIMULATION RESULTS FOR AC SYSTEM FAULTS

Fault location	Bus voltage (p.u.)	W_R (Mvar*s)	W_I (Mvar*s)	Fault identification result
AC system fault in rectifier side	0.2	-0.6987	-1.6742	External faults
	0.5	-0.3816	-0.8186	
	0.7	-0.0862	-0.2135	
AC system fault in inverter side	0.2	19.6954	13.0323	External faults
	0.5	22.0830	17.1084	
	0.7	24.8851	16.5022	

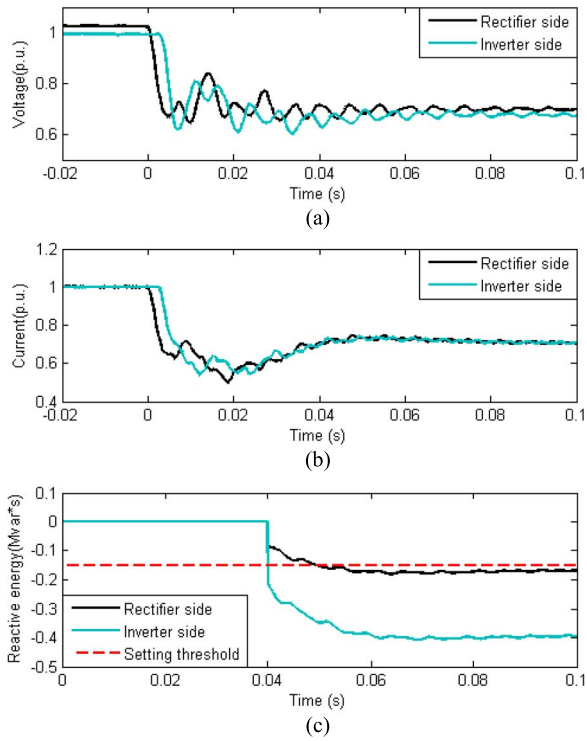

Fig. 9. Simulation results of an ac system fault with a bus voltage of 0.7 p.u. (a) Voltage. (b) Current. (c) Reactive energy.

AC System Faults: AC system faults with different voltage dips are further tested. The faults are located at F_4 and F_5 in Fig. 5(a), and reactive energy results at 0.04 s are listed in Table II. The faults are observed as external faults, except for the 0.7-p.u. voltage dip at the rectifier side, at which the reactive energy of the rectifier side is less than the threshold at 0.04 s. The simulation results in Fig. 9 further clarify this case. At 0.049 s, the reactive energy exceeds the threshold, and the external fault is correctly identified.

Load Variation: Power regulation of the dc line will cause transient processes that may activate the protection system. Hence, load variations of the dc line are considered in this study to test the robustness of the proposed scheme. Different load current varying ranges are simulated, and the results calculated at 0.04 s are tabulated in Table III. When the load fluctuates over small ranges, the reactive energies are less than the threshold during the entire protection time and, thus, the variation is regarded as a disturbance. During situations with large fluctuations in the load, the reactive energy exceeds the

TABLE III
SIMULATION RESULTS FOR LOAD VARIATION SITUATIONS

Current change (p.u.)	W_R (Mvar*s)	W_I (Mvar*s)	Fault identification result
0.1	0.0113	0.0037	
0.2	0.0515	0.0183	Disturbances
0.3	0.1278	0.0473	
0.5	0.4155	0.1536	External faults

TABLE IV
SIMULATION RESULTS FOR DIFFERENT FAULT DISTANCE SITUATIONS

Fault distance from rectifier side (km)	W_R (Mvar*s)	W_I (Mvar*s)	Fault identification result
1	4.4206	-1.6212	
100	3.4133	-1.5282	
200	3.5828	-1.3372	
400	3.8290	-1.1483	Internal faults
600	7.3303	-1.1054	
700	6.7181	-1.2031	
799	7.4823	-3.4486	

threshold and initiates the fault direction identification procedure. However, the reactive energy directions of both sides are the same, so an external fault is recognized.

In summary, the proposed protection scheme is adaptive to various types of faults and disturbances and it is able to correctly and rapidly identify internal faults.

C. Influence of Fault Distance

Fault distances are set from 1 to 799 km in the 800-km dc line to test the effectiveness of the proposed protection. The results in Table IV indicate that when the fault distance varies, the reactive energies at 0.04 s are larger than the threshold, and their directions are opposite. Thus, internal faults are recognized. The protection still correctly identifies the faults even in close-up and distant fault situations.

D. Influence of Fault Resistance

Sensitivity is an important factor in evaluating protection schemes. To verify the sensitivity, fault resistance is set from 0 to 200 Ω at the midpoint of the dc transmission line. The reactive energies varying with the fault resistances are shown in Fig. 10. The reactive energies at both sides decrease with increasing fault resistance, indicating that the protection becomes less sensitive. Nevertheless, the values of the reactive energies remain larger than the threshold and, thus, the proposed protection still performs effectively even in conditions of high ground resistance of 200 Ω.

E. Influence of the Sampling Frequency

Table V shows the simulation results for various sampling frequencies with a positive pole fault at the midpoint of the transmission line. As shown, the calculated reactive energies are not significantly affected by the sampling frequency. The correct directions of the reactive energies are still derived even for a low sampling frequency of 1 kHz. Therefore, a high sampling frequency is not necessary under this protection scheme, making it more practical in implementation.

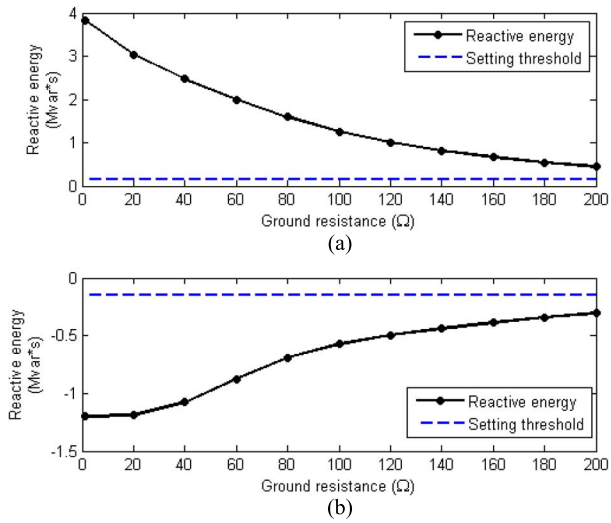

Fig. 10. Reactive energies for various fault resistances. (a) Rectifier side. (b) Inverter side.

TABLE V
SIMULATION RESULTS FOR VARIOUS SAMPLING FREQUENCIES

Sampling frequency (kHz)	W_R (Mvar*s)	W_I (Mvar*s)	Fault identification result
20	3.7981	-1.1349	
10	3.8290	-1.1483	
5	3.8935	-1.1772	Internal faults
1	4.0015	-1.1542	

TABLE VI
PARAMETERS OF THE SIMULATION SYSTEM

Symbol	Description	Value
U_N	The rated voltage	500 kV
I_N	The rated current	2 kA
U_{s1}	AC system	2.5@84 deg, 345 kV, 50 Hz
U_{s2}	AC system	2.5@75 deg, 230 kV, 50 Hz
Z_S	Smoothing reactor	0.29 H
X_l	The leakage reactance of the converter transformer	0.18 p.u.
L	DC line length	800 km
R	Line resistance	0.0396 Ω/km
C_1		2 μF
L_1		11.71 mH
C_2		9.074 μF
L_2	DC filter	5.874 mH
C_3		2 μF
L_3		6.46 mH
C_4		3.752 μF
L_4		11.35 mH

V. CONCLUSION

This paper proposes a novel protection algorithm based on reactive energies for HVDC transmission lines. The Hilbert transform is employed to calculate the reactive energy, which ensures the continuous outcome of the reactive energy and fault direction during the entire time of protection. The characteristics of the reactive energy under various fault conditions are analyzed based on the equivalent circuit of the HVDC system and applied to construct the direction protection.

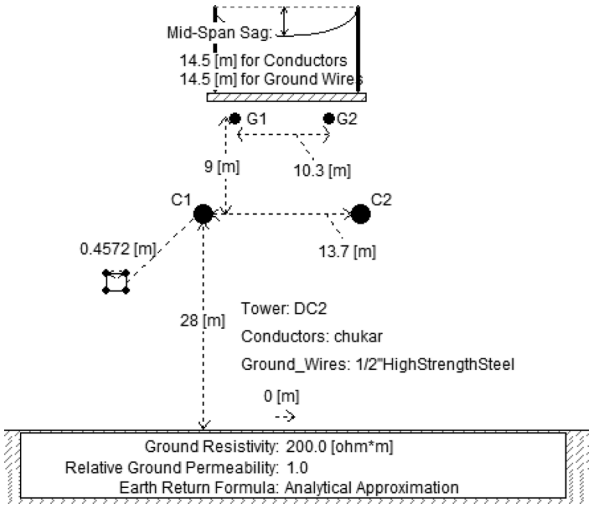

Fig. 11. Tower data of the HVDC transmission line.

Extensive simulations are conducted to verify the effectiveness of the protection scheme. The proposed protection scheme correctly distinguishes the faults under all test conditions, including internal faults, external faults, ac faults, load variations, and fault distance variations. Compared to current differential protection, this protection induces a smaller time delay, thus significantly accelerating fault detection. Moreover, the protection is adaptive to fault resistances, which guarantees protection sensitivity. Moreover, the reactive energy calculation is not sensitive to the sampling frequency and, therefore, a low sampling frequency can be used to improve its applicability. In summary, the proposed protection scheme exhibits good performance under various situations and is feasible for further applications.

APPENDIX

The parameters of the HVDC system are listed in Table VI. The tower parameters of the HVDC transmission-line model are shown in Fig. 11.

REFERENCES

[1] W. Long and S. Nilsson, "HVDC transmission: Yesterday and today," *IEEE Power Energy Mag.*, vol. 5, no. 2, pp. 22–31, Mar. 2007.
[2] P. Bresesti, W. L. Kling, R. L. Hendriks, and R. Vailati, "HVDC connection of offshore wind farms to the transmission system," *IEEE Trans. Energy Convers.*, vol. 22, no. 1, pp. 37–43, Mar. 2007.
[3] P. M. Anderson, "HVDC protection," in *Power System Protection*. Hoboken, NJ, USA: Wiley, 1998, pp. 913–954.
[4] Y. Zhang, N. Tai, and B. Xu, "Fault analysis and traveling-wave protection scheme for bipolar HVDC lines," *IEEE Trans. Power Del.*, vol. 27, no. 3, pp. 1583–1591, Jul. 2012.
[5] D. Naidoo and N. M. Ijumba, "A protection system for long HVDC transmission lines," in *Proc. IEEE Power Eng. Soc. Inaugural Conf. Expo. Africa*, Durban, South Africa, 2005, pp. 150–155.
[6] X. Liu, A. H. Osman, and O. P. Malik, "Hybrid traveling wave/boundary protection for monopolar HVDC line," *IEEE Trans. Power Del.*, vol. 24, no. 2, pp. 569–578, Apr. 2009.
[7] X. Liu, A. H. Osman, and O. P. Malik, "Real-time implementation of a hybrid protection scheme for bipolar HVDC line using FPGA," *IEEE Trans. Power Del.*, vol. 26, no. 1, pp. 101–108, Jan. 2011.
[8] J. Suonan, J. Zhang, Z. Jiao, L. Yang, and G. Song, "Distance protection for HVDC transmission lines considering frequency-dependent parameters," *IEEE Trans. Power Del.*, vol. 28, no. 2, pp. 723–732, Apr. 2013.
[9] G. Wang, M. Wu, H. Li, and C. Hong, "Transient based protection for HVDC lines using wavelet-multiresolution signal decomposition," in *Proc. IEEE/PES Transmission Distrib. Conf. Exhibit.: Asia Pacific*, Dalian, China, 2005, pp. 1–4.
[10] X. Zheng, N. Tai, J. S. Thorp, and G. Yang, "A transient harmonic current protection scheme for HVDC transmission line," *IEEE Trans. Power Del.*, vol. 27, no. 4, pp. 2278–2285, Oct. 2012.
[11] G. Song, X. Chu, S. Gao, X. Kang, and Z. Jiao, "A new whole-line quick-action protection principle for HVDC transmission lines using one-end current," *IEEE Trans. Power Del.*, vol. 30, no. 2, pp. 599–607, Apr. 2015.
[12] H. Takeda, H. Ayakawa, M. Tsumenaga, and M. Sanpei, "New protection method for HVDC lines including cables," *IEEE Trans. Power Del.*, vol. 10, no. 4, pp. 2035–2039, Oct. 1995.
[13] A. Li, Z. Cai, Q. Sun, X. Li, D. Ren, and Z. Yang, "Study on the dynamic performance characteristics of HVDC control and protections for the HVDC line fault," in *Proc. Power Energy Soc. Gen. Meeting*, Calgary, AB, Canada, 2009, pp. 1–5.
[14] *IEEE Guide for the Analysis and Definition of DC-Side Harmonic Performance of HVDC Transmission Systems*, IEEE Standard 1124, 2003.
[15] C. K. Kim, V. K. Sood, G. S. Jang, S. J. Lim, and S. J. Lee, "Control of HVDC converter and system," in *HVDC Transmission: Power Conversion Applications in Power Systems*. Hoboken, NJ, USA: Wiley, 2009, pp. 97–148.
[16] A. D. Poularikas, "Hilbert transforms," in *Transforms and Applications Handbook*, 3rd ed. Boca Raton, FL, USA: CRC, 2010, pp. 7.1–7.100.
[17] T. Cui, X. Dong, Z. Bo, and A. Juszczyk, "Hilbert-transform-based transient/intermittent earth fault detection in noneffectively grounded distribution systems," *IEEE Trans. Power Del.*, vol. 26, no. 1, pp. 143–151, Jan. 2011.
[18] F. Luo, J. Li, Z. Xu, Y. Li, J. Zhang, and S. Liu, "Study on impedance-frequency characteristics of HVDC filter commutate converter," in *Proc. 3rd Int. Conf. Dereg. Restruct. Power Technol.*, Nanjing, China, 2008, pp. 1652–1656.
[19] Y. Ma, X. Xiao, X. Jiang, and Y. Zhao, "Study on impedance-frequency characteristic of HVDC converter," *Autom. Elect. Power Syst.*, vol. 30, no. 12, pp. 66–69, Jun. 2006.
[20] CIGRE Working Group B4.45, "Technological assessment of 800 kV HVDC applications," CIGRE Tech. Brochure 417, Jun. 2010.
[21] *IEEE Guide for Power System Protective Relay Applications Over Digital Communication Channels*, IEEE Standard C37.236, 2013.
[22] M. Szechtman, T. Wess, and C. V. Thio, "First benchmark model for HVDC control studies," *Electra*, no. 135, pp. 54–73, Apr. 1991.
[23] *"PSCAD/EMTDC User's Manual,"* Manitoba HVDC Research Center, Winnipeg, MB, Canada, 2003.
[24] J. R. Marti, "Accurate modelling of frequency-dependent transmission lines in electromagnetic transient simulations," *IEEE Trans. Power App. Syst.*, vol. PAS-101, no. 1, pp. 147–157, Jan. 1982.

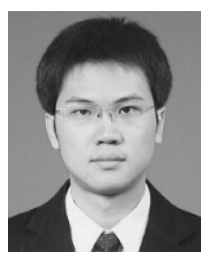

Shuxin Luo (S'15) was born in Guangdong, China, in 1987. He received the B.Sc. degree in electrical engineering from Tsinghua University, Beijing, China, in 2010, where he is currently pursuing the Ph.D. degree in electrical engineering.

His main research interests are power system protection and HVDC protection.

Xinzhou Dong (M'99–SM'01) was born in Shaanxi, China, in 1963. He received the B.Sc., M.Sc., and Ph.D. degrees in electrical engineering from Xi'an Jiaotong University, Xi'an, China, in 1983, 1991, and 1996, respectively.

He furthered his postdoctoral research at the Electrical Engineering Station of Tianjin University, Tianjin, China, from 1997 to 1998. Since 1999, he has been with Tsinghua University, Beijing, China. Currently, he is a Professor with the Department of Electrical Engineering, Tsinghua University, and Director of the International Union Research Center of Beijing on Green Energy and Power Safety. He is an author or co-author of more than 200 journal papers. His research interests include protective relaying, fault location, and the application of wavelet transforms in power systems.

Prof. Dong is a fellow of IET.

Shenxing Shi (M'08) was born in Jiangsu, China, in 1978. He received the B.Sc. degree in electrical engineering from Northeast Electric Power University, Jilin, China, in 1999, and the Ph.D. degree in electrical engineering from Tsinghua University, Beijing, China, in 2006.

Currently, he is an Associate Professor with the Department of Electrical Engineering, Tsinghua University, Beijing, China. His research interests include traveling-wave-based protective relaying and fault analysis in power systems.

Bin Wang (M'09) was born in Shandong, China, in 1978. He received the B.Sc. and Ph.D. degrees in electrical engineering from Shandong University of Technology, Shandong, in 1999 and 2005, respectively.

Currently, he is an Associate Professor with the Department of Electrical Engineering, Tsinghua University, Beijing, China. His main research interests are power system protection, digital substation automation, and power quality.